In Situ Surface-Enhanced IR Absorption Spectroscopy on CO Adducts of Iron Protoporphyrin IX Self-Assembled on a Au Electrode

Min Ma,[†] Yan-Gang Yan,[†] Sheng-Juan Huo,[†] Qun-Jie Xu,[‡] and Wen-Bin Cai*[,†,‡]

Shanghai Key Laboratory for Molecular Catalysis and Innovative Materials and Department of Chemistry, Fudan University, Shanghai 200433, China, and Department of Environmental Engineering, Shanghai University of Electric Power, Shanghai 200090, China

Received: March 30, 2006; In Final Form: June 12, 2006

The surface coordination chemistry of carbon monoxide with the reduced form ($Fe^{II}PP$) of iron(III) protoporphyrin IX ($Fe^{III}PP$) monolayer self-assembled on a Au electrode in 0.1 M $HClO_4$ was studied for the first time by using in situ ATR-surface-enhanced infrared absorption spectroscopy (ATR-SEIRAS). Both mono- and biscarbonyl adducts [simplified as $Fe^{II}(CO)PP$ and $Fe^{II}(CO)_2PP$, respectively] were detected, depending on the history of potential control. Initially, the $Fe^{II}(CO)PP$ predominates, and the intermediate transition potential for the conversion of $Fe^{II}(CO)PP$ to $Fe^{III}PP$ and CO was spectrally determined to be ca. 0.09 V (vs SCE). The ratio of $Fe^{II}(CO)_2PP$ and $Fe^{II}(CO)PP$ increases after a potential excursion to a sufficiently positive value. $Fe^{II}(CO)_2PP$ is much more stable against its electro-oxidation to $Fe^{III}PP$ than its counterpart $Fe^{II}(CO)PP$ with increasing potential. The observed change of coordination properties may be ascribed to an irreversible structural reorganization of the FePP adlayer caused by the potential excursion.

Introduction

The coordination chemistry of CO with metalloporphyrins is a biologically and chemically important topic as promoted by the interest in comparing the coordination properties of metalloporphyrins with those of heme proteins. Historically, studies on CO binding with metalloporphyrins were mainly limited to bulk-phase reactions.[1] There is a growing trend for surface electrochemists to confine such prototype coordination reactions at electrodes, with the expectation that such efforts may help to create or modify versatile functional solid−liquid interfaces.

Iron(III) protoporphyrin IX ($Fe^{III}PP$) or hemin self-assembled or immobilized on graphite, glassy carbon, and metal surfaces exhibits excellent electrocatalysis toward the reduction of dioxygen,[2a,b] hydrogen peroxide,[2a,b] nitrite,[2c] and carbon dioxide[2d] as well as potential sensing capabilities for trace amounts of CO and NO.[2e,f] A recent report suggests that a strong electronic coupling between an FePP molecule and a metal could be relevant in the perspective of being exploited in the building of hybrid nanodevices.[3] The structure and electronic property of the hemin-adlayer-modified electrodes have been studied by conventional electrochemical methods,[2b] STM,[4a] UV−vis reflectance spectroscopy (UVRS),[4b] and surface-enhanced (resonance) Raman spectroscopy (SERS or SERRS).[4c−e] On the basis of STM and UVRS measurement, self-assembled FePP monolayer on HOPG electrode has been proposed to be oriented with its porphyrin ring lying nearly flat or slightly tilted on the surface.[4a,b] SERS or SERRS has been applied to characterize the oxidized and reduced forms of hemin adlayers[4c−e] as well as nitrosyl adducts[2e] on ORC-roughened Ag electrodes. As for the surface coordination by NO, unfortunately no direct internal NO stretching band was observed by SERS with the 532 nm laser as the excitation radiation, and the formation of nitrosyl adducts of $Fe^{III}PP$ can only be judged by the change in relative intensities of porphyrin ring bands.[2e] This is probably because of a much lower Raman scattering cross section for this small and highly polar ligand molecule. Similarly, it can be expected that SERS may not be suitable for the characterization of surface coordination of CO to $Fe^{II}PP$, either. The main difference of these two ligand molecules is that NO is capable of binding to both $Fe^{II}PP$ and $Fe^{III}PP$, whereas CO can only bind to $Fe^{II}PP$.

Surface infrared spectroscopy is more suitable for direct detection of the internal stretching vibration of small molecules with large dipole moments. In particular, ATR-surface-enhanced IR absorption spectroscopy (ATR-SEIRAS) merits higher surface sensitivity and less interference from the bulk solution as compared to that of conventional infrared reflection absorption spectroscopy (IRAS), thus facilitating in situ monitoring of surface adsorption and reaction.[5,6] To our knowledge, surface coordination of CO to an $Fe^{II}PP$ adlayer on an electrode surface has not been investigated spectroscopically. In this report, we will demonstrate the formation and breakage of carbonyl adducts of an $Fe^{II}PP$ adlayer on a Au electrode as a function of potential by taking the advantage of in situ ATR-SEIRAS. We will show that the potential excursion may change the distribution of two types of carbonyl adducts on the Au electrode.

Experimental Section

A SEIRA-active Au nanoparticle film (ca. 60 nm thick) was prepared on the total-reflecting plane of a hemicylindrical Si prism with the electroless plating method.[6b−e] After being thoroughly rinsed with ultrapure Milli-Q water, the Au film was immersed in a 50 μM iron(III) protoporphyrin IX ($Fe^{III}PP$) (Aldrich Chemical Co.) in 0.1 M Borax solution overnight for self-assembly. The Au film was then thoroughly rinsed again with ultrapure water and assembled into a spectroelectrochemical cell with a Krestchmann ATR configuration (a prism/Au film

* Corresponding author. Phone: +86-21-55664050. Fax: +86-21-65641740. E-mail: wbcai@fudan.edu.cn.
[†] Fudan University.
[‡] Shanghai University of Electric Power.

10.1021/jp061962g CCC: $33.50
Published on Web 07/13/2006

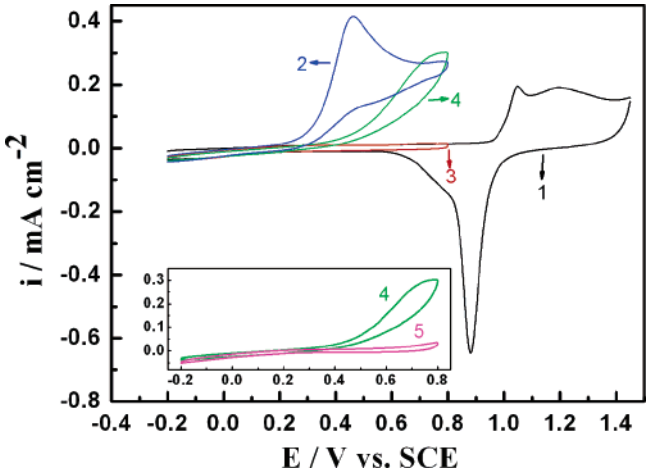

Figure 1. Cyclic voltammograms for a bare Au electrode in neat 0.1 M $HClO_4$ (trace 1) and CO-saturated 0.1 M $HClO_4$ (trace 2) and for an FePP-immobilized Au electrode in neat 0.1 M $HClO_4$ (trace 3) and CO-saturated 0.1 M $HClO_4$ (trace 4). Inset: cyclic voltammograms for a CO-predosed FePP-immobilized Au electrode in the presence (trace 4) and the absence (trace 5) of solution CO. Initial and final potentials, −0.2 V; upper potential limits, 1.45 V (trace 1) and 0.8 V (the other traces); scan rate, 50 mV s^{-1}.

(working electrode)/solution geometry). A Magna-IR E. S. P. System 760 FT-IR (Nicolet) equipped with a liquid nitrogen cooled MCT detector was used to acquire in situ ATR-SEIRAS spectra. Unpolarized radiation passed through the Si prism and hit the Au/electrolyte interface at an incident angle of 65°, and the reflected beam was detected with an MCT detector. The spectral resolution was set to 4 cm^{-1}. All the spectra were shown in the absorbance unit defined as $-\log(I/I_0)$, where I and I_0 represent single-beam spectra taken at the sample and reference potential, respectively. Spectral analysis was carried out with the Grams 32 software package (Galactic, Inc.).

All the (spectro)electrochemical measurements on the Au working electrode were carried out in 0.1 M $HClO_4$ with the potential controlled by a CHI660B electrochemistry workstation and with a Pt sheet and a saturated calomel electrode serving as the counter and reference electrode, respectively. All the potentials were quoted against a saturated calomel electrode (SCE). Before measurements, the electrolyte was purged with a high-purity Ar flow for at least 1 h.

Results and Discussion

Voltammetric Behaviors. The wide-ranged cyclic voltammogram (trace 1) recorded for the bare Au film electrode in 0.1 M $HClO_4$ between −0.2 and 1.45 V is shown in Figure 1, where the oxidative and reductive voltammetric response is typical of a polycrystalline Au electrode. Also shown in Figure 1 are narrow-ranged cyclic voltammograms between −0.2 and 0.8 V recorded for the FePP-modified Au electrode in neat 0.1 M $HClO_4$ (trace 3) and CO-saturated 0.1 M $HClO_4$ (trace 4), as well as the bare Au electrode in CO-saturated 0.1 M $HClO_4$ (trace 2). In neat 0.1 M $HClO_4$, no clear redox peaks can be found for the FePP-modified Au except a slight reduction of double-layer charging current as compared to that of the bare Au electrode. The nearly featureless redox behavior is similar to that observed for an FePP-modified Ag electrode, in stark contrast to FePP-modified PG electrodes, which may reflect relatively sluggish electron transfer between the central Fe(III) of FePP and the metal. It is not clear whether the strong electronic coupling between FePP and the metal as revealed by SERS study may contribute to the above redox behavior.

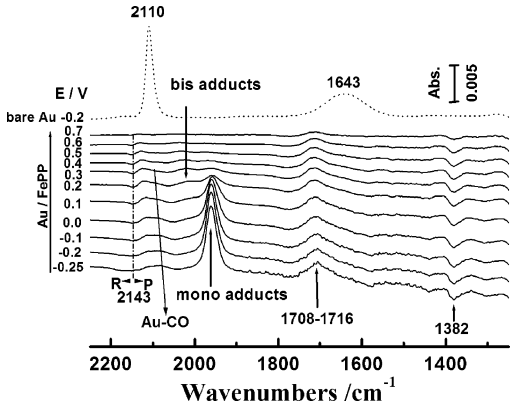

Figure 2. Potential-dependent ATR-SEIRA spectra for an FePP SAM modified Au electrode in CO-saturated 0.1 M $HClO_4$. The reference spectrum was taken at 0.8 V. The arrow on the left indicates the sequence of the sample spectra taken at various potentials. For comparison, the ATR-SEIRA spectrum for a bare Au electrode at −0.2 V in otherwise the same measurement conditions is given (top curve). The 2143 cm^{-1} band indicated is due to a trace amount of gaseous CO, and the Au−CO band around 2100 cm^{-1} is due to CO linearly adsorbed on exposed Au sites.

Nevertheless, significant difference in the oxidative current peaks for the bare Au (trace 2) and the FePP-modified Au (trace 4) electrode can be found in CO-saturated 0.1 M $HClO_4$. Not only does the oxidative process shift to a higher potential, but also the oxidation current is significantly reduced. For a bare Au electrode, the oxidation wave in trace 2 was attributed to superposition of the oxidation of solution CO and adsorbed CO.[6f] Cyclic voltammograms of an FePP-modified Au electrode before and after solution CO removal are compared (see inset of Figure 1), indicating rather featureless current response for the latter in the potential region of interest. CO adducted to the $Fe^{II}PP$ adlayer should decoordinate as its central Fe(II) ion was oxidized to Fe(III) ion, different from the direct electro-oxidation of CO adsorbed on a metal electrode. Obviously, in trace 4 the presence of an FePP adlayer hinders the underlying active Au sites in the oxidation of solution CO as well as CO adsorbed on exposed Au. The FePP adlayer can be destroyed and even removed from the surface by oxidation if the potential sweeps to higher potentials (not shown).

In Situ SEIRAS Measurement. It should be noted that in the irreversible adsorbed FePP adlayer on Au in pH 1 solution, only monomeric FePP forms.[4e,7] Figure 2 shows potential-dependent ATR-SEIRA spectra of a freshly prepared FePP adlayer on a Au electrode in CO-saturated 0.1 M $HClO_4$. The higher surface sensitivity of ATR-SEIRAS versus that of conventional IRAS is beneficial to yield the above good-quality spectra (see the Supporting Information for an evaluation of S/N ratios of these two measurement modes). For comparison, ATR-SEIRA spectrum for a chemically deposited bare Au film on Si in CO-saturated 0.1 M $HClO_4$ at −0.2 V is displayed on the top trace of Figure 2, exhibiting one linearly adsorbed CO band around 2100 cm^{-1}, close to that reported previously.[6e,f] Upon being modified with an FePP adlayer, this band greatly weakens and shifts slightly to lower frequencies as compared to that for a bare Au electrode, which is in accordance to the voltammetric behavior as shown in Figure 1. Also noted is a weak band for gaseous CO centered at 2143 cm^{-1} consisting of P and R branches, which may be caused by slight fluctuation of CO bubbling in maintaining a saturated CO in 0.1 M $HClO_4$ during the process of measurement. This band can be completely removed after Ar purging for 1 h as can be seen later in Figure 5 and also in the Supporting Information.

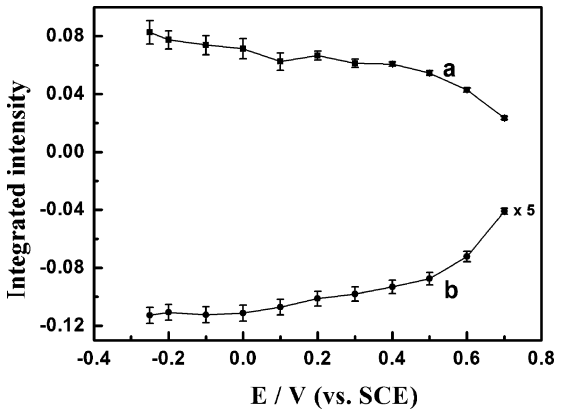

Figure 3. Plots of the integrated intensities for the band at ca. 1710 cm^{-1} (a) and the band at 1382 cm^{-1} (b) shown in Figure 2 as a function of potential. Integrated band intensities and error bars were obtained by using curve-fitting procedures in Grams 32. Deconvolution analysis was applied to subtract a minor interfacial water band from the C═O stretching band. The band intensity in plot b has been magnified by 5.

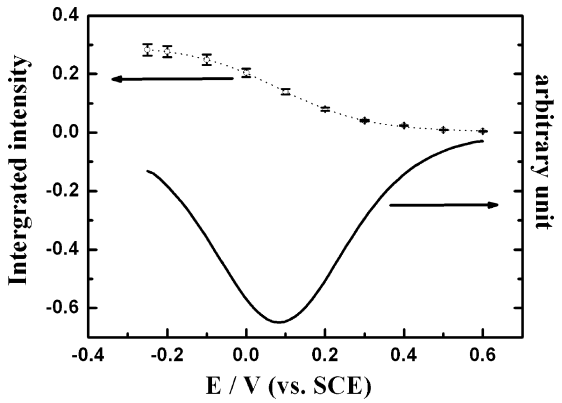

Figure 4. Plot of integrated intensity of the 1960 cm^{-1} band (from Figure 2) vs potential (open circles) and the arbitrary fitting curve (dashed line); the peak-shaped curves in this figure represent the derivatives of the adsorption isotherm for the FePP obtained from best fits to the experimental data.

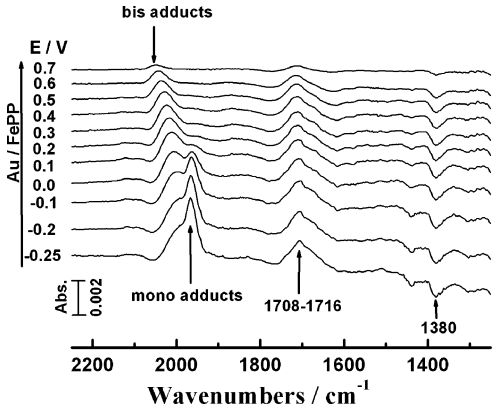

Figure 5. Potential-dependent ATR-SEIRA spectra reacquired for an FePP-modified Au electrode after the potential excursion to 0.80 V as described in Figure 2. The electrode was kept again at −0.20 V in CO-saturated 0.1 M $HClO_4$ for 10 min followed by removal of CO with Ar bubbling for 1 h, before initiating a second-round multistep ATR-SEIRA spectra acquisition. The reference spectrum was acquired at 0.80 V. The arrow on the left indicates the sequence of sample spectra taken at various potentials.

Due to the roughly D_{4h} symmetry of the FePP molecules, SERS-active bands for porphyrin skeletal vibrations did not show up in SEIRAS. The upward band at 1708−1716 cm^{-1} and the downward band at 1382 cm^{-1} can be assigned to the carbonyl vibration ($\nu_{C=O}$) of the peripheral propionic group and the symmetric carboxylate vibration (ν_{O-C-O}) of the peripheral propionate group.[6c,8] The intensity versus potential plots for these two bands is shown in Figure 3. Relatively slow intensity changes are observed for the 1710 cm^{-1} and 1382 cm^{-1} bands in the potential range of −0.25 to 0.50 V, respectively, followed by a more drastic decrease (increase) in intensity for the former (latter) as the potential moves further positively. Two carboxylic groups are contained in a nominal FePP molecule; for the adsorbed FePP molecule in acidic solution of pH 1, at least one carboxylic group loses a proton upon anchoring to the Au surface through the carboxylate oxygen atoms with a bridging coordination at the reference potential of 0.8 V as indicated by the negative-going band at 1382 cm^{-1}. From the above observation, we deduce that the orientation of adsorbed FePP adlayer does not change significantly between −0.25 and 0.5 V, at least not to an extent to which a substantial CO coordination change may occur. On the basis of STM and UV−vis measurement of FePP on a HOPG electrode,[4a,b] FePP molecules may assume a nearly flat or slightly tilted orientation on the Au electrode as well at lower potentials. At potentials positive of ca. 0.5 V, the porphyrin ring may reorientate to a relatively large extent by tilting up the ring plane through anchoring a carboxylate group on the metal surface. Similar potential-induced depronation and reorientation have been reported for other carboxylic-group-containing molecules such as *p*-nitrobenzoic acid and benzoic acid on a Au electrode as the potential moves positively.[6c,8b,c] This structural change of the FePP adlayer upon the above potential excursion could be irreversible, leaving sufficient steric space for the formation of both mono- and biscarbonyl adduct when the FePP adlayer was reduced back (vide infra).

It is well-known from previous study on bulk-phase metalloporphyrin complexes that $Fe^{II}PP$ can form both mono- and biscarbonyl adducts of iron and ruthenium porphyrins.[9,10] The band frequency falls between ca. 1920−1975 cm^{-1} for the former and 1990−2050 cm^{-1} for the latter, and the frequency depends on the kinds of central metal ions, the trans base ligands, and the peripheral structures of the porphyrins.[10] The higher C−O stretching frequencies for the biscarbonyl complexes can be explained in terms of diminished π back-bonding resulting from the two carbonyl functions competing for the central metal d-orbitals.

The most important feature in Figure 2 is the appearance of a strong band located around 1960 cm^{-1} in the lower potential range. The infrared frequency is very close to ν_{CO} of the monocarbonyl ligand of other model iron porphyrin compounds, such as FeTPP, and hence can be assigned to ν_{CO} of the CO ligand coordinated to the Fe(II) ion of the reduced form Fe^{II}-PP.[11] The nearly flat orientation of FePP at lower potentials favors the formation of the monocarbonyl adduct, as the formation of biscarbonyl adducts is largely hindered by steric factors. Previous SERS results on FePP on an ORC-roughened Ag electrode by Cai et al. in the absence of CO suggests that the FePP adlayer adapts four-coordination and intermediate spin.[4e] Therefore, five-coordinate Fe^{II}(CO)PP is the most likely species for the surface monocarbonyl adduct. Since CO does not combine with the oxidized form of FePP (or Fe^{III}PP),[10] the intensity of the 1960 cm^{-1} band decreases with increasing potential as the transformation of Fe(II) to Fe(III) in the FePP adlayer proceeds, via

$$Fe^{II}(CO)PP = Fe^{III}PP + CO + e^{-} \quad (1)$$

The decoordinated CO may either diffuse into the bulk solution

or undergo further oxidation to CO_2, depending on the potential applied. Nevertheless, since CO oxidation at a bare Au surface initiates at around 0.25 V (see Figure 1) at which most of the adducted CO molecules are already decoordinated from the FePP adlayer (see Figure 2), diffusion of decoordinated CO into the bulk solution at these lower potentials is more likely. Figure 4 plots the variation of CO band intensity for the monocarbonyl adduct as a function of potential (open circles), which corresponds to a potential-dependent adsorption isotherm specifically for the FePP adlayer on a Au electrode in CO-saturated 0.1 M $HClO_4$ solution. Also displayed in this figure is a statistical fit to the experimental data (dashed line), which upon differentiation produced a peak-shaped curve analogous to the expected, redox-based voltammetric response (solid line). The peak potential at ca. 0.09 V (vs SCE) corresponds approximately to the intermediate transition potential of the surface reaction as suggested in eq 1.

For a vacuum-evaporated bare Au nanofilm on Si in CO-saturated 0.1 M $HClO_4$, a rather weak band around 2000−2050 cm^{-1} can be identified, in addition to a major band above 2100 cm^{-1}. The former band was ascribed to CO linearly adsorbed on special sites of Au/Si interfaces, and it disappeared as the CO in solution was removed with Ar purging.[6f] For a chemically deposited bare Au nanofilm electrode in a CO-saturated 0.1 M $HClO_4$ solution, only the latter band can be detected,[6e] as shown in the uppermost spectrum of Figure 2. Since the chemically deposited Au nanofilm was used for the current study, the very weak (or barely identifiable) shoulder band around 2030 cm^{-1} for the FePP-modified Au electrode can be reasonably assigned to the presence of a trace amount of biscarbonyl adduct of Fe^{II}-PP, a definitely minor species due to the above-mentioned steric hindrance.

The spectral pattern obtained for a CO-predosed Fe^{II}PP-modified Au electrode in the absence of solution CO is essentially similar to that in the presence of CO. However, the following is noted: first, after purging solution CO, the CO band at −0.2 V decreases a bit; second, the intermediate oxidation potential of Fe^{II}(CO)PP to Fe^{III}PP shifts negatively; third, the weak band for gaseous CO molecules disappears after purging solution CO (see the Supporting Information).

The relative band intensity of the above two types of carbonyl adducts varies with the structural change of the FePP adlayer after potential excursion. Shown in Figure 5 are multistep SEIRA spectra reacquired for the same electrode from −0.25 to 0.8 V after the first-round potential-dependent spectra were acquired as shown in Figure 2. Before the reacquisition, the potential was reset to −0.2 V in the presence of CO-saturated 0.1 M $HClO_4$ for 10 min followed by bubbling Ar to purge solution CO for 60 min. For bulk phase coordination reactions of other iron porphyrin molecules, the coordination constant of a monocarbonyl adduct is higher than its corresponding biscarbonyl adduct; as a result, the five-coordinate monocarbonyl adduct will convert to the six-coordinate biscarbonyl adduct with increasing CO pressure,[9a,11] and the opposite process will take place with decreasing CO pressure. For the surface CO coordination to an FePP adlayer at a Au electrode, at least in the time domain of the measurement, the purging of solution CO does not cause a significant reduction in the IR bands for these two species for the same electrode, which is suggestive of rather strong coordination affinity of CO to the FePP adlayer on the Au electrode. This situation largely resembles that found for the CO adlayer on a Pt group or an Fe group metal electrode.[6b,12]

In stark contrast to that found in Figure 2, the band for the biscarbonyl adduct of Fe^{II}PP increased tremendously accompanied with a decrease in the band for the monocarbonyl adduct of Fe^{II}PP. We assume that the increase of the biscarbonyl ν_{CO} band is due to irreversible structural reorganization of the FePP adlayer after the positive potential excursion to 0.8 V. As we mentioned earlier there exists significant potential-dependent reorientation of FePP molecules at potentials higher than 0.5 V, which may allow the tilting-up of the porphyrin macrocycle plane. Upon returning the potential to −0.2 V, not all adsorbed FePP molecules resume the same nearly flat orientation on Au as the original one; the ratio of up-tilting FePP molecules to flat-lying ones at lower potentials increases as compared to that in the first round. This up-tilting orientation leaves open space for CO to coordinate to the central Fe(II) iron from both sides of a porphyrin macrocycle plane, forming a six-coordinate biscarbonyl adduct, whereas the other Fe^{II}PP species with a flat orientation has only one side of the macrocycle plane open to form a five-coordinate monocarbonyl adduct. In contrast to the monocarbonyl adduct, the biscarbonyl adduct is much more stable against the increasing potential as suggested by the presence of a downward lobe on the higher frequency side of this absorption band at lower potentials with the reference spectrum taken at 0.8 V.

Unlike the CO adsorbed on a metal electrode where CO per se is directly electro-oxidized to CO_2 at positive potentials, in the present case CO decoordinates from the FePP adlayer as the electro-oxidation of its Fe(II) to Fe(III) proceeds with increasing potential. The difference in the electro-oxidation of Fe(II) to Fe(III) for the above two types of FePP species can at least be partly explained in terms of their structural difference, i.e., the central Fe(II) ion of a nearly flat-lying five-coordinate Fe^{II}PP species is closer to the Au electrode surface and therefore is more facile for electron transfer than that of a up-tilting six-coordinate one. The reason the potential induced a larger stark tuning rate for the biscarbonyl adduct (ca. 60 cm^{-1}/V) than for the monocarbonyl adduct (less than 10 cm^{-1}/V) is not clear right now and deserves further study.

Conclusion

In situ SEIRAS has been applied to study the coordination of CO with the reduced form of an iron(III) protoporphyrin IX adlayer self-assembled on a Au electrode in 0.1 M $HClO_4$ as a function of potential control. Initially, the monocarbonyl adduct species predominate at negative potentials, and the intermediate transition potential for the oxidation of Fe^{II}(CO)PP to Fe^{III}PP + CO was spectrally determined to be ca. 0.09 V (vs SCE). The ratio of bis- versus monocarbonyl adducts increases after a potential excursion to a sufficiently positive value. In contrast to the monocarbonyl adduct, the biscarbonyl adduct stabilizes the central metal ion Fe(II) tremendously against its electro-oxidation to Fe(III). An irreversible structural reorganization of the FePP adlayer may explain the above behavior.

Acknowledgment. The ATR Si prism was a gift from Professor M. Osawa in the Catalysis Research Center, Hokkaido University. External IRAS measurement was assisted by Professor Xin-Hua Xia, Nanjing University. The NSFC (No. 20473025), the SRFDP (No. 20040246008), the NCET (No. 04-0349), and the SNPC (No. 0452nm064-2) are gratefully acknowledged for financial support. Y.Y.G. appreciates the support of the Innovation Fund from Fudan University (No. CQH 1615018). We also thank the State Key Laboratory for Physical Chemistry of Solid Surfaces, Xiamen University (No. 200303) for providing partial financial support and technical assistance.

Supporting Information Available: Figures showing ATR-SEIRAS with CO-predosed Fe^{II}PP-modified Au electrode, normalized intensities as a function of potential, and integrated intensities as a function of potential and the Appendix. This material is available free of charge via the Internet at http://pubs.acs.org.

References and Notes

(1) (a) Swistak, C.; Kadish, K. M. *Inorg. Chem*. **1987**, *26*, 405. (b) Komatsu, T.; Ohmichi, N.; Nakagawa, A.; Zunszain, P. A.; Curry, S.; Tsuchida, E. *J. Am. Chem. Soc*. **2005**, *127*, 15933.

(2) (a) Jiang, R. Z.; Dong, S. J. *Electrochim. Acta* **1990**, *35*, 1227. (b)Shigehara, K.; Anson, F. C. *J. Phys. Chem.* **1982**, *86*, 2776. (c) Mimica, D.; Zagal, J. H.; Bedioui, F. *J. Electroanal. Chem*. **2001**, *497*, 106. (d) Gao, Y.; Chen, J. *J. Electroanal. Chem*. **2005**, *583*, 286. (e) Shi, Q. F.; Cai, W. B.; Scherson, D. A. *J. Phys. Chem. B* **2004**, *108*, 17281. (f) Bedioui, F.; Villeneuve, N. *Electroanalysis* **2003**, *15*, 5.

(3) (a) Bizzarri, A. R.; Cannistraro, S. *J. Phys. Chem. B* **2005**, *109*, 16571. (b) Liu, Z. M.; Yasseri, A. A.; Lindsey, J. S.; Bocian, D. F. *Science* **2003**, *302*, 1543.

(4) (a) Tao, N. J.; Cardenas, G.; Cunha, F.; Shi, Z. *Langmuir* 1**996**, *11*, 4445. (b) Sagara, T.; Fukuda, N.; Nakashima, N. *J. Phys. Chem. B* **1998**, *102*, 521. (c) McMahon, J. J.; Baer, S.; Melendres, C. A. *J. Phys. Chem*. **1986**, *90*, 1572. (d) Sanchez, L. A.; Spiro, T. G. *J. Phys. Chem.* **1985**, *89*, 763. (e) Cai, W. B.; Stefan, I. C.; Scherson, D. A. *J. Electroanal. Chem*. **2002**, *524*−*525*, 36.

(5) (a) Bjerke, A. E.; Griffiths, P. R.; Theiss, W. *Anal. Chem.* **1999**, *71*, 1967. (b) Shao, M. H.; Adzic, R. R. *J. Phys. Chem. B* **2005**, *109*, 16563. (c) Wandlowski, Th.; Ataka, K.; Pronkin, S.; Diesing, D. *Electrochim. Acta* **2004**, *49*, 1233. (d) Yajima, T.; Uchida, H.; Watanabe, M. *J. Phys. Chem. B* **2004**, *108*, 2654. (e) Futamata, M.; Luo, L. Q.; Nishihara, C. *Surf. Sci.* **2005**, *590*, 196.

(6) (a) Osawa, M. In *Handbook of Vibrational Spectroscopy*; Chalmers, J. M., Griffiths, P. R., Eds.; John Wiley & Sons: Chichester, U.K., 2002; Vol. 1, p 785. (b) Yan, Y. G.; Li, Q. X.; Huo, S. J.; Ma, M.; Cai, W. B.; Osawa, M. *J. Phys. Chem. B* **2005**, *109*, 7900. (c) Huo, S. J.; Li, Q. X.; Yan, Y. G.; Chen, Y.; Cai, W. B.; Xu, Q. J.; Osawa, M. *J. Phys. Chem. B* **2005**, *109*, 15985. (d) Huo, S. J.; Xue, X. K.; Yan, Y. G.; Li, Q. X.; Ma, M.; Cai, W. B.; Xu, Q. J.; Osawa, M. *J. Phys. Chem. B* **2006**, *110*, 4162. (e) Miyake, H.; Ye, S.; Osawa, M. *Electrochem. Commun*. **2002**, *4*, 973. (f) Sun, S. G.; Cai, W. B.; Wan, L. J.; Osawa, M. *J. Phys. Chem. B* **1999**, *103*, 2460.

(7) Yoshimoto, S.; Yokoo, N.; Fukuda, T.; Kobayashi, N.; Itaya, K. *Chem. Commun.* **2006**, *5*, 500.

(8) (a) Zhang, Z. J.; Imae, T. *Nano Lett.* **2001**, *1*, 241. (b) Królikowska, A.; Kudelski, A.; Michota, A.; Bukowska, J. *Surf. Sci.* **2003**, *532*−*535*, 227. (c) Ikezawa, Y.; Sekiguchi, R.; Kitazume, T. *Electrochim. Acta* **2000**, *46*, 731.

(9) (a) Wayland, B. B.; Mehne, L. F.; Swartz, J. *J. Am. Chem. Soc*. **1978**, *100*, 2379. (b) Krim, L.; Sorgues, S.; Soep, B.; Shafizadeh, N. *J. Phys. Chem. A* **2005**, *109*, 8268.

(10) Yu, N.-T.; Kerr, E. A. In *Biological Applications of Raman Spectroscopy*; Spiro, T. G., Ed.; John Wiley and Sons: New York, 1986; Vol. 2, p 55.

(11) Struass, S. H.; Holm, R. H. *Inorg. Chem*. **1982**, *21*, 863.

(12) Guesta, A.; Gutiérrez, C. *J. Phys. Chem.* **1996**, *100*, 12600.